Genome-wide analysis of phased nucleosomal arrays reveals the functional characteristic of the nucleosome remodeler ACF

Dhawal S. Jain[1], Sandro Baldi[1], Angelika Zabel[1], Tobias Straub[2]* and Peter B. Becker[1]*

[1]Molecular Biology and [2]Bioinformatics Units,
Biomedical Center and Center for Integrated Protein Science Munich
Ludwig-Maximilians-University, Planegg-Martinsried, Germany

*Correspondence
Peter B. Becker: email: pbecker@med.uni-muenchen.de
Tel: +49(0)89-2180-75427

Tobias Straub: email: tstraub@med.uni-muenchen.de
Tel: +49(0)89-2180-75439

Keywords: Chromatin; nucleosome remodeling; linker DNA; regularity; Micrococcal nuclease;

Abstract

The nature of chromatin as regular succession of nucleosomes has gained iconic status. The average nucleosome repeat length (NRL) determined by classical means serves as index for bulk chromatin of a given specimen. However, this value is dominated by regular heterochromatin since nucleosomal arrays are often not regular at individual single copy sequences.

To obtain a measure for nucleosome regularity in euchromatin we subjected nucleosome profiles of *D. melanogaster* embryos to autocorrelation and spectral density estimation. These revealed variation in nucleosome regularity and NRL at different types of euchromatin and yielded a comprehensive catalog of regular phased nucleosome arrays (PNA). The absence of the nucleosome sliding factor ACF1 correlated with global loss of regularity and increased NRL in euchromatin and specifically compromised phasing at a novel class of PNA. Our approach is generally applicable to characterize the functional diversification of nucleosome remodelers in euchromatin organization.

Introduction

Chromatin evolved for optimal packaging of eukaryotic DNA. It ensures protection of genomes from environmental damage while granting dynamic access to the genetic information as needed. Histone octamers wrap DNA segments of about 146 bp thus forming nucleosomes, the ever-repeating fundamental unit of chromatin. Active regulatory regions, such as promoters and enhancers, are devoid of nucleosomes. In general, nucleosome-depleted regions (NDR) must be carefully managed, since free DNA poses the risk of breakage or unwarranted activity involving underlying DNA (Struhl and Segal 2013; Becker and Workman 2013; Peterson and Almouzni 2013).

Neighboring nucleosomes are separated by variable lengths of linker DNA, which provides binding sites for linker histones, remodeling factors and other DNA binding proteins. Average linker lengths between nucleosomes – their spacing – can be measured in bulk chromatin by partial cleavage of linker DNA with Micrococcal Nuclease (MNase). The fact that the average nucleosome repeat length (NRL) varies depending on species, cell type, functional chromatin state and chromosomal position (Teif et al. 2012; Valouev et al. 2011; Sperling and Weiss 1980; Sperling et al. 1980; Omori et al. 1980; Berkowitz and Riggs 1981; Jakob et al. 1984; Szerlong and Hansen 2011; Igo-Kemenes et al. 1982; Zlatanova et al. 1999) shows that a continuum of chromatin structures are compatible with genome functions. Indeed, numerous observations suggest that the regularity of nucleosome spacing varies considerably along the chromosome. For example, inactive heterochromatic domains that package repetitive DNA show extensive regularity while the extent of nucleosome spacing in euchromatin is more variable (Wallrath and Elgin 1995; Sugiyama et al. 2007; Sun et al. 2001; Mavrich et al. 2008). Conceivably, the regular nucleosome spacing is disrupted in active chromatin due to the many remodeling events associated with the usage of chromatin as a template for transcription, replication and repair processes.

The regularity of nucleosomal arrays is best appreciated at chromosomal loci where nucleosome positions are put in register by a DNA sequence or protein boundary that operates in all cells. A prominent example is the alignment of nucleosomes to the NDRs that characterize transcription start sites (TSS). In *Drosophila*, the first few nucleosomes just downstream of TSSs are particularly well positioned with defined spacing (Mavrich et al. 2008; Sala et al. 2011), a situation referred to as 'regular nucleosome phasing'. The precise placement of the first downstream (+1) nucleosome bears regulatory potential in the context of initiation and promoter release of RNA polymerase II (Lieleg et al. 2015b; Soboleva et al. 2014; Weber and Henikoff 2014; Gilchrist and Adelman 2012). The extent with which nucleosomes are positioned with respect to DNA sequence at other sites in the *Drosophila* genome is unclear to date, due to the lack of suitable methodology to identify phased nucleosomes (Gaffney et al. 2012).

Although the benefits of charge neutralization in chromatin may lead to statistical alignment of nucleosomes close to a boundary structure (Fedor et al. 1988), it is now clear that nucleosome spacing and their phasing are active processes, brought about by so-called nucleosome remodeling enzymes. These enzymes bind substrate nucleosomes and disrupt histone-DNA contacts by cycles of ATP hydrolysis-driven conformation changes (Mueller-Planitz et al. 2013; Narlikar et al. 2013). Modulations of these remodeling reactions may lead to displacement of histone octamers along DNA (their sliding), or to the reversible eviction of histones (Clapier and Cairns 2009). The prominent example of yeast chromatin impressively documents the specialization of various remodeling factors for positioning nucleosomes downstream of TSSs (Iyer 2012; Struhl and Segal 2013; Valouev et al. 2011; Yen et al. 2012; Ganguli et al. 2014; Krietenstein et al. 2016). To which extent the alignment of nucleosomes to other types of chromatin boundaries depends on remodeling factors is largely unknown.

We are interested in the closely related remodeling complexes ACF and CHRAC. These conserved remodeling enzymes consist of the ATPase ISWI and the large ACF1 subunit. Association of two small histone fold proteins with ACF constitutes CHRAC (Corona et al. 2000; Hartlepp et al. 2005; Poot et al. 2000; Kukimoto et al. 2004). CHRAC and ACF are prototypic nucleosome sliding factors that are able to catalyze the alignment of adjacent nucleosomes with respect to each other. Their ability to 'space' nucleosomes into arrays in the absence of boundaries has been thoroughly characterized *in vitro* (Torigoe et al. 2011; Hwang et al. 2014; Ito et al. 1997; Varga-Weisz et al. 1997). Remarkably, the ISWI-containing nucleosome remodeling factor NURF, which also catalyzes nucleosome sliding, does not promote regular nucleosome spacing, but rather disrupts regular nucleosome arrays (Tsukiyama et al. 1995; Tsukiyama and Wu 1995). These early observations revealed that ISWI's nucleosome sliding activity may be harnessed by associated factors to achieve different goals (Mueller-Planitz et al. 2013; Clapier and Cairns 2009).

Despite the presumed most fundamental importance of ACF/CHRAC for chromatin organization, little is known about their global activities in physiological chromatin. Since both factors are thought to catalyze similar reactions, we and others have studied flies bearing mutations in the ACF1 gene to score their combined phenotypes (Fyodorov et al. 2004; Chioda et al. 2010). Early on, defects in bulk nucleosome spacing have been reported for the *acf1*^{1} mutant allele (Fyodorov et al. 2004). However, we recently observed that this allele does not represent a clean loss of function but may arise from the out-of-context

expression of a C-terminal ACF1 fragment (Börner et al. 2016). We also recently characterized a novel null allele, *acf1*^{7}, which has clear morphogenesis phenotypes in *Drosophila* oogenesis (Börner et al. 2016).

To reveal the contributions of CHRAC/ACF to nucleosome spacing and positioning *in vivo* we globally compared nucleosome spacing and phasing in euchromatin of wild type *Drosophila* embryos with chromatin of ACF1-deficient embryos. At first sight global nucleosome occupancy and placement does not change much. However, applying spectral density estimation to reveal the underlying periodicity in nucleosome occupancy patterns reveals that ACF1 deletion leads to reduced regular nucleosome phasing at large numbers of specific sites. The presence of a defined sequence motif at these genomic loci suggests that ACF aligns nucleosomes to a boundary, the nature of which is yet to be defined. By contrast, depletion of NURF did not affect nucleosome phasing at these sites. Autocorrelation of the nucleosomal map reveals that CHRAC/ACF restricts nucleosome spacing to physiological distances throughout euchromatin. Depletion of ACF1 does not affect the regular phasing of nucleosomes at transcriptional start sites documenting the functional diversification of remodeling factors.

Results

Nucleosome occupancy and phasing in *Drosophila* embryos

In order to study the effects of ACF1 depletion on nucleosome occupancy and positioning we first generated reference maps using two different *Drosophila* strains, *yw* and *w1118*, which are wild type (WT) with respect to the *Acf1* gene. Nuclei of 2-8 hr old embryos were digested with MNase to yield predominantly mononucleosomes (Supplementary Fig. 1a). We obtained 5 consistent high quality nucleosome occupancy profiles from independent WT samples (Fig. 1, Supplementary Fig 1a-c).

The regularity of nucleosomal arrays can be best appreciated if they are phased by alignment to a DNA sequence or protein boundary that operates in all cells. A prominent example of this kind is the regular phasing of nucleosome arrays with respect to promoter NDRs. In order to comprehensively reveal phased arrays in the *Drosophila* genome we applied spectral density estimation to sliding 1 kb windows along the nucleosome dyad density profiles. The method treats nucleosome occupancy as a composite periodic signal and decomposes it into a linear combination of simple periodic functions using Fourier transformation. The weights (or spectral densities) and periods of the decomposed functions determine the overall contribution of a given period to the composite pattern. Accordingly, phased regular nucleosomal arrays (PNA) are revealed by dominant weight of a period that conforms to the positioning of equally spaced nucleosomes.

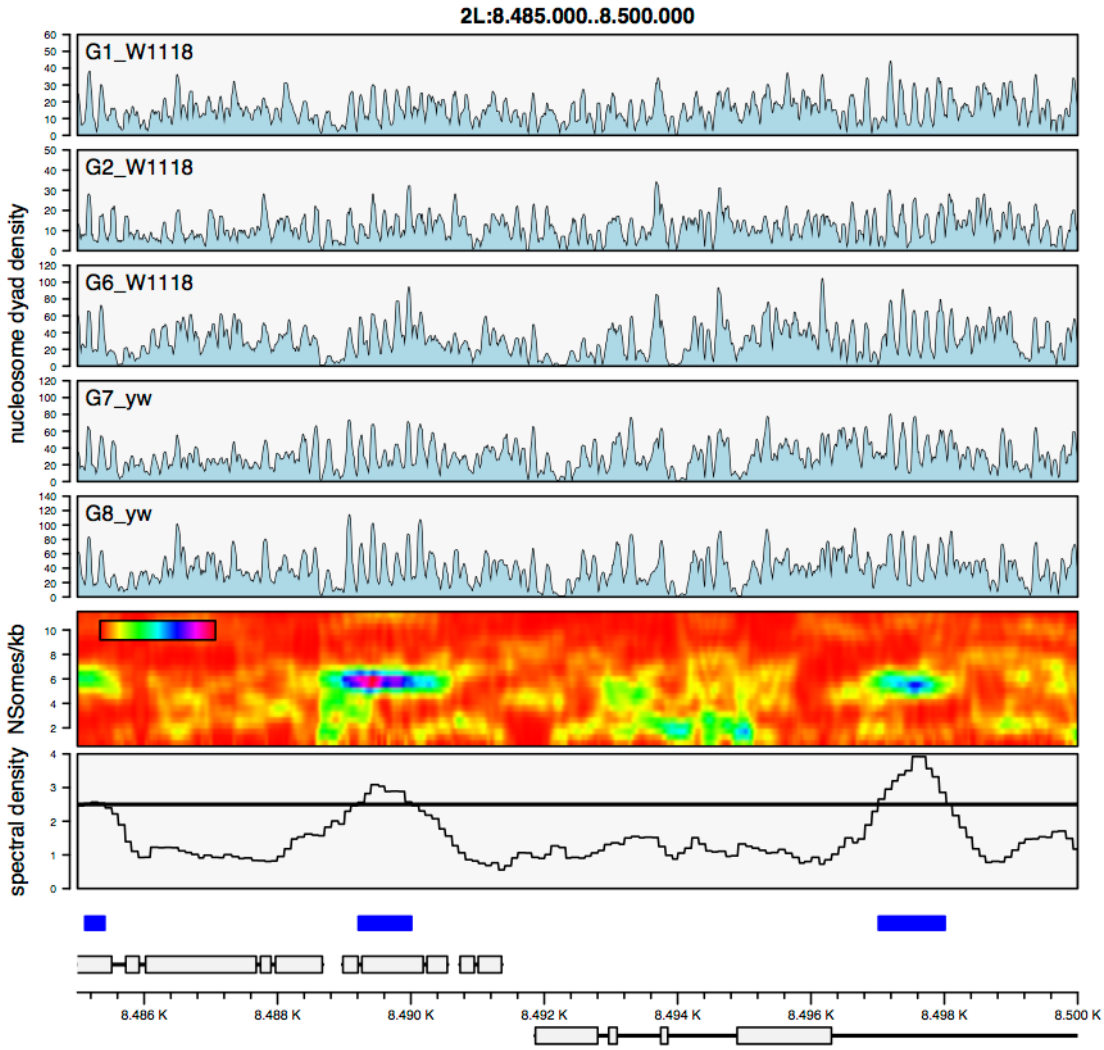

Figure 1: Identification of phased nucleosome arrays (PNA) Nucleosome dyad densities for a representative genomic region are displayed for 5 WT samples of two different genotypes (upper panels). Heat map: spectral densities obtained from sample "G8_yw" are displayed for the range of 1-11 nucleosomes per kb (periods of 100-500 bp). Lower panel: Spectral density corresponding to a frequency of 5.2 nucleosomes per 1kb (repeat length 193 bp) after standardization and averaging across all the samples. An arbitrary threshold set at 2.5 defines phased nucleosome arrays (PNA) that are displayed as blue boxes below the trace.

The heatmap panel in Fig. 1 provides an exemplary spectral decomposition in a genomic window of 15 kb. PNA are revealed by the weight of a periodicity in the dyad density profiles corresponding to a physiological nucleosome density of roughly 5-6 nucleosomes per 1000 bp. For a genome-wide identification of such regions we applied an arbitrary threshold to the average spectral density of above-mentioned periodicity in our WT profiles and obtained 10,417 regions with a median length of 700 bp, accounting for 6.2% of the euchromatin fraction of the genome (Supplementary Table 1). These regions are enriched 2.7 fold at promoters and are correspondingly enriched 5.1 fold in 'state 1' chromatin, which characterizes active promoters (Kharchenko et al. 2011) (Fig. 2a, b). This observation agrees with the known strong nucleosome phasing adjacent to NDRs at promoter regions.

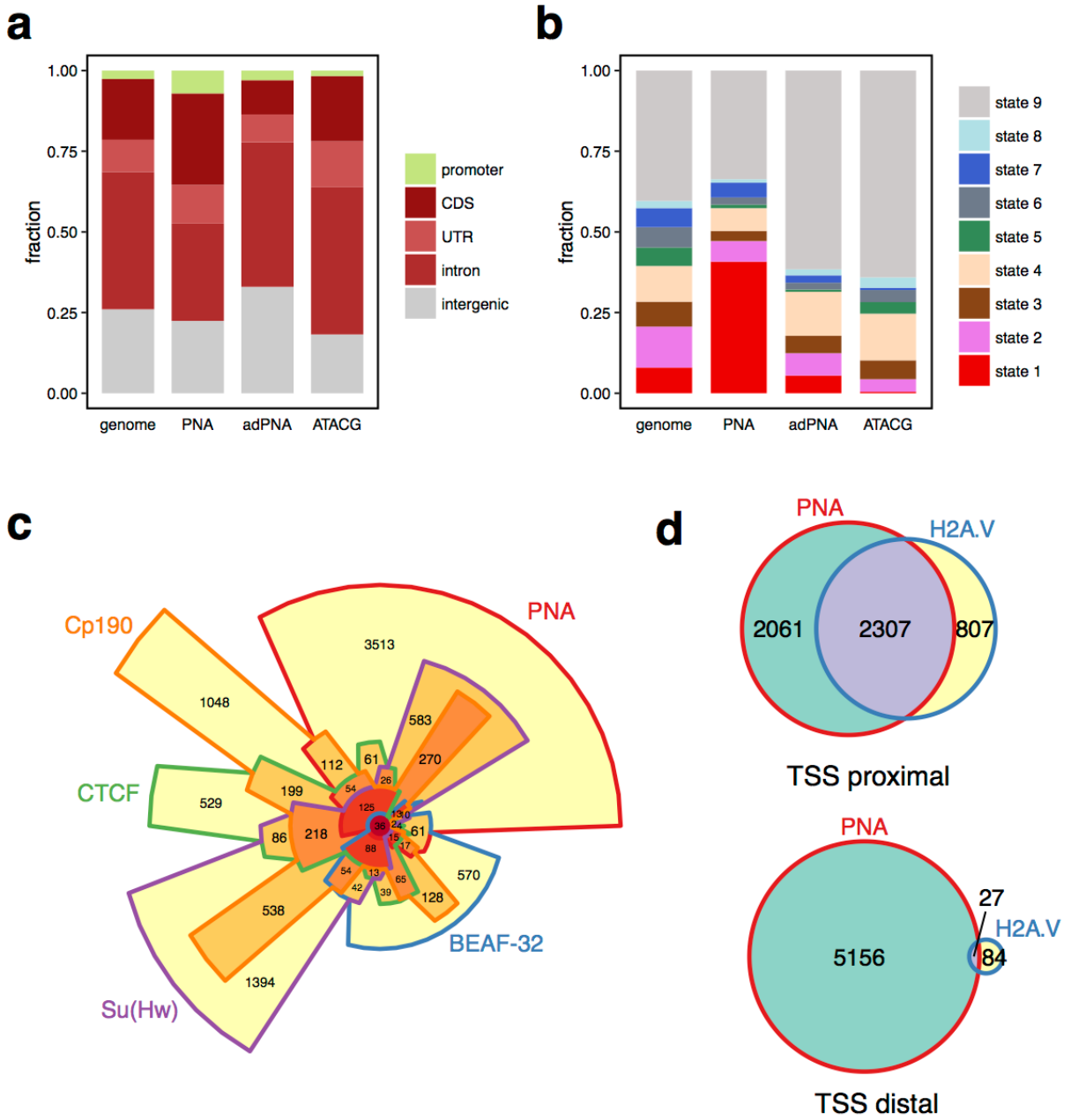

Figure 2: **Genome-wide distribution of phased nucleosomal arrays (PNA)**. (a) Genomic feature annotation and (b) chromatin state distribution of PNA regions (n=10417), ACF1-dependent phased nucleosomal arrays (adPNA, n=1624), and ATACG motif hits (ATACG, n=3031). The overall feature distribution in the genome is provided for comparison. (c) Overlap of PNA with various insulator proteins in genomic regions distal to TSS (>1000 bp distance, n=5190). Insulator peaks were based on modENCODE maps (Celniker et al. 2009) in *Drosophila* embryos. (d) Overlap of PNA with H2A.V enrichment regions in TSS proximal (upper panel) and distal regions (lower panel).

5190 PNA were found localized at least 1 kb away from TSS with close to random distribution with respect to the underlying chromatin state-annotation. According to earlier reports the chromatin interaction of insulator proteins, such as BEAF32, CTCF, Su(Hw) or CP190, may constitute a boundary that leads to nucleosome phasing(Fu et al. 2008; Cuddapah et al. 2009). About 70% of the PNAs distal to TSS, however, were not overlapping with ChIP-seq peaks of these proteins (Fig 2c). In contrast to phased nucleosome arrays next to promoter NDRs, we did not find the histone variant H2A.V particularly enriched at these non-TSS phased arrays (Fig 2d).

Genes overlapping with non-TSS PNA have varied levels of transcriptional activity across development, ranging from ubiquitous expression to largely no activity, when compared to the entire developmental transcriptome database of *Drosophila* (Graveley et al. 2011) (not shown).

In summary, our spectral density analysis identified numerous regions of nucleosome phasing. About half of those co-localize with TSS. The majority of nucleosomal arrays distal to TSS are not explained by known phasing principles such as boundaries posed by insulator proteins.

ACF1-containing remodeling factors contribute to nucleosome phasing at specific sites

The generation of PNA at the boundaries posed by promoter NDRs is facilitated by ATP-dependent nucleosome remodeling factors (Struhl and Segal 2013; Lieleg et al. 2015b; Yen et al. 2012; Iyer 2012; Ganguli et al. 2014). Since nucleosome sliding factors CHRAC/ACF, which share the signature subunit ACF1, have not been assessed for their roles in the generation of PNA, we mapped nucleosome occupancies in *acf1*^{7} mutant embryos (Börner et al. 2016). Overall, we obtained fewer sequencing reads than for the WT samples (an average of 78×10^6 in WT and 52×10^6 in *acf1*^{7}). However, the fragment size distribution, the cumulative nucleosome dyad densities along TSS and the distribution of dyads along the genome for each sample were very similar (Supplementary Fig. 1a-c).

We determined the PNA in the mutant background using triplicate dyad density profiles. Using t-statistics we then identified 1624 regions with reduced nucleosome phasing in the *acf1* mutant embryos, which we refer to as ‘ACF1-dependent phased nucleosomal arrays’ (adPNA) sites (Fig. 3, Supplementary Table 2). ACF1 does not contribute to regular nucleosome phasing at TSS, an observation that provides convenient internal controls for adPNA sites, which are found predominantly in intronic and intergenic regions (Fig. 2a). Likewise, phasing at CTCF boundary sites is not affected by depletion of ACF1 (Supplementary Fig. 2a)

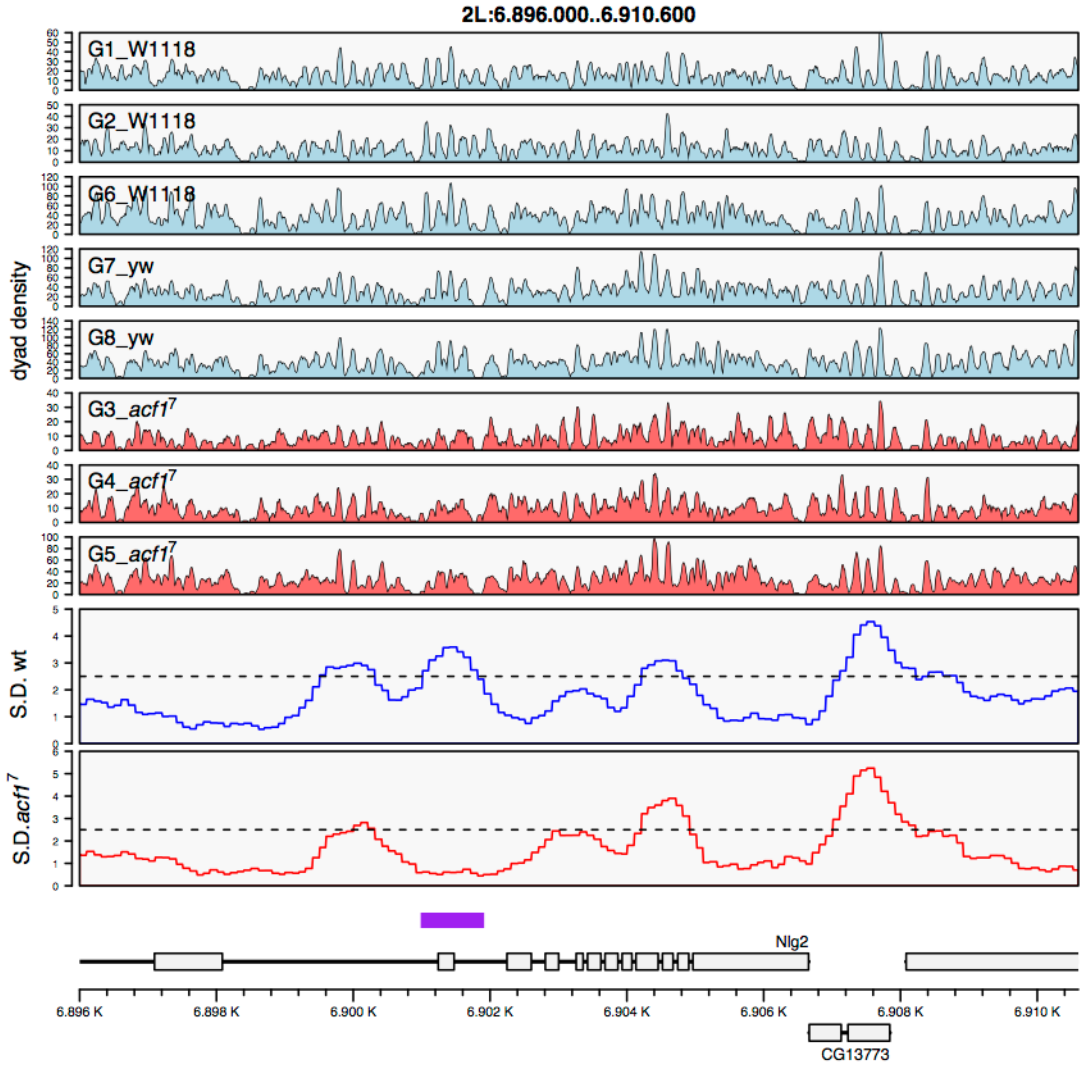

Figure 3: Identification of ACF1-dependent phased nucleosome arrays (adPNA). WT (red) and acf17 (cyan) tracks of nucleosome dyad densities for all biological replicates. The average spectral density (S.D.) for 193 bp repeat length is displayed for both WT and acf17 genotypes. adPNA sites (purple bar) were identified using Welch t-test statistics with multiple testing correction (FDR < 5%) on the standardized spectral densities.

The reduced nucleosome phasing in the *acf1*^{7} mutant is not confounded by lower nucleosome occupancy. Comparison of library size-normalized fragment counts along the adPNA sites in WT and mutant using DESeq2 (Love et al. 2014) suggests similar fragment densities (not shown). Furthermore, assessment of nucleosome densities per gene or per 200 bp non-overlapping windows across the genome in WT and *acf1*^{7} background does not show major differences (not shown).

In order to reveal shared sequence features among all adPNA sites we identified DNA motifs *de novo* using MEME (Bailey et al. 2009). Interestingly, a complex signature characterized by an ATACG motif was present in >75% of the adPNA sites (Fig. 4a, Supplementary Text). The motif showed no similarity to known ones in the JASPAR database (Mathelier et al. 2014).

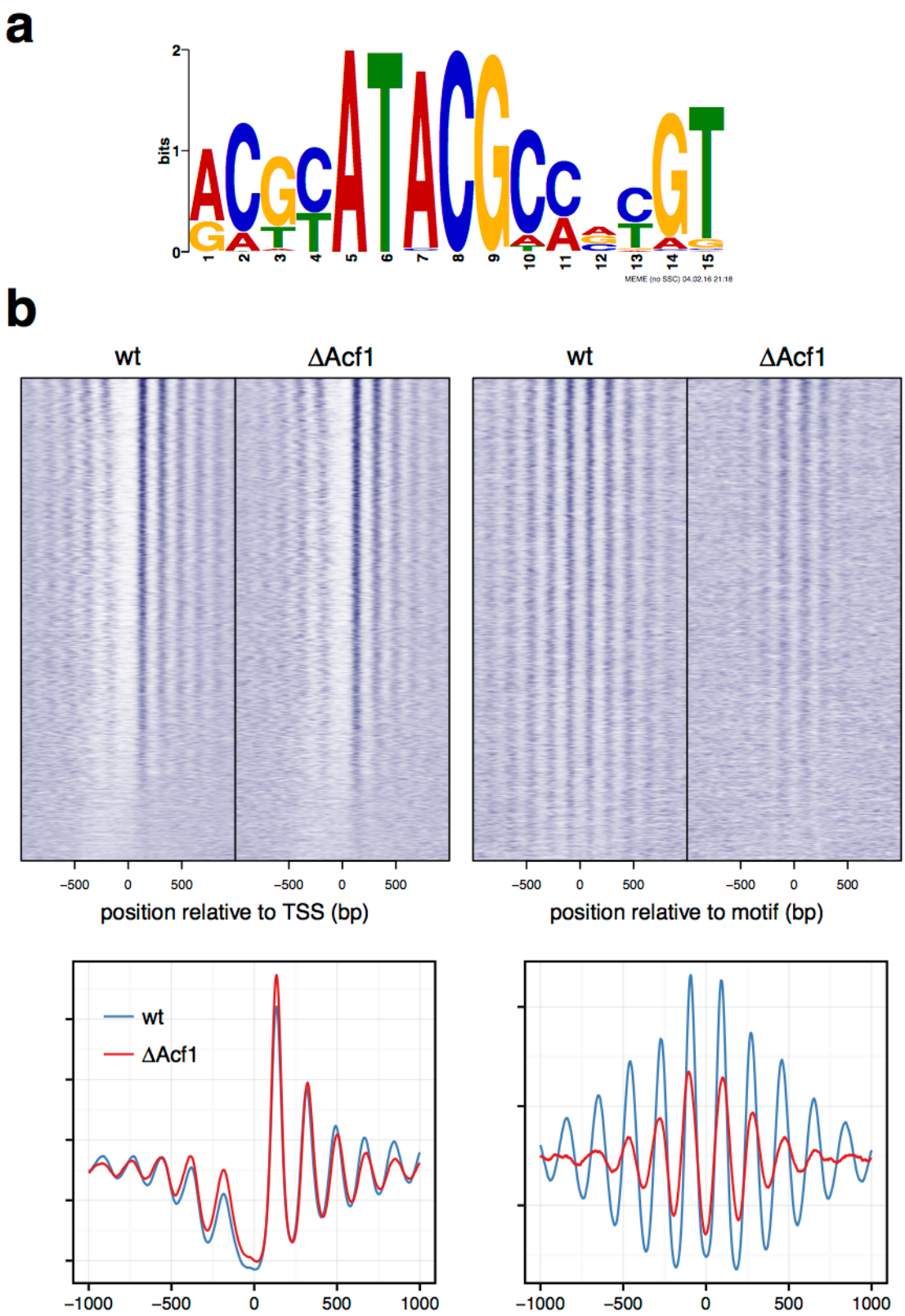

Figure 4 Organization of nucleosomes around the ATACG motif. (a) Motif enriched in adPNAs (E-value 4.2e-2420). (b) Upper panels: Nucleosome dyad densities were obtained in 2 kb windows centered around the TSS of the top 50% expressed genes in 2-8 hr old embryos (left) or the 3031 ATACG motif instances (right). Heatmap representation of all instances sorted decreasingly based on their spectral density at 193 bp repeat length. Lower panels: Corresponding average plots for WT and acf17 mutants.

Sequences that conform with the ATACG consensus motif are found at 3031 sites in the genome with a p-value $<10^{-7}$. Cumulative plots of nucleosome positions centered at ATACG sites reveals very regular

nucleosome phasing in WT chromatin, which becomes fuzzy upon the deletion of ACF1. Remarkably, regular phasing was as well defined as that at TSS, which was not affected by deletion of ACF1 (Fig. 4b). The ATACG motif is invariably localized in the central linker of small arrays consisting of 8-10 regularly phased nucleosomes. In contrast to PNA around TSS and insulator binding sites, we do not observe nucleosome depletion on the motif hits. Consistent with this finding, analysis of nucleosome positioning potential using the NuPoP package at ATACG motifs sites suggests that they do not particularly disfavor nucleosome assembly. These sites also do not correspond to enhancer regions, since comparison to the published enhancer inventories obtained through STARR-seq or genome-wide contact frequency maps (Hi-C)(Arnold et al. 2013; Sexton et al. 2012) only yielded a very poor overlap (<7% of the queried intervals). A similarly poor match was found if ATACG motif sites were compared to a list of recently mapped DNA replication origins (Comoglio et al. 2015) (data not shown).

ATACG motifs are found throughout the genome (Fig. 2a). Comparison to the 9-state chromatin annotation reveals that 64% of the motif regions are localized within the silent ‘state 9’ chromatin. Of note, active TSS corresponding to state 1 are almost devoid of these motifs (Fig. 2b).

Interestingly, the adPNA sites or ATACG motif regions have been conserved during the evolution of insect genomes. The PhastCons score calculated by alignments of 15 insect genomes allows to determine the base conservation probability along queried intervals (Siepel et al. 2005). The degree of conservation at 1 kb intervals centered around adPNA sites or ATACG motif regions was higher compared to the poorly conserved introns and intergenic regions in general (Supplementary Fig. 2b).

The reduced phasing of nucleosomes around ATACG motifs suggests a direct role for ACF/CHRAC in nucleosome alignment. Unfortunately, a physical interaction of ACF1 with these sites cannot be documented by ChIP, presumably due to the poor crosslinking of the remodeler to chromatin (Jain et al. 2015).

We wished to explore whether ACF1 was unique in its ability to phase nucleosomes at ATACG motifs or whether this was a more general property of ISWI-containing nucleosomes sliding factors. Recently, Badenhorst and colleagues (Kwon et al. 2016a) presented a comprehensive analysis of the NURF-dependent nucleosome positioning changes. We assessed nucleosomal array formation (Fig. S3) in this data set at the same reference points (TSS, CTCF sites, ATACG motifs) analysed in our ACF samples (Figs. 4b/S2a). In *NURF301* mutant samples nucleosome phasing at TSS and CTCF sites was diminished , but regularity flanking the ATACG motif was unchanged. We conclude that phasing at ATACG sites is a specific property of ACF, and hence the name adPNA sites appropriate.

Autocorrelation analysis reveals a global role for ACF1 in nucleosome spacing

Cumulative plotting of nucleosome dyads downstream of TSSs and around ATACG sites suggested that the nucleosome spacing becomes slightly wider in the absence of ACF1 (Fig. 4b). To quantitatively determine changes in nucleosome repeat length (NRL), we applied the autocorrelation function on the nucleosome dyad density pattern. The periodic maxima in the curves reflect the underlying periodicities

in nucleosome organization (Braunschweig et al. 2009). In a genome-wide analysis comprising chromosomes 2 and 3 (Fig. 5a), a significant dampening of the autocorrelation amplitudes was observed, which revealed that in general the NRL is less regular along the entire length of the chromosome in the absence of the remodeler.

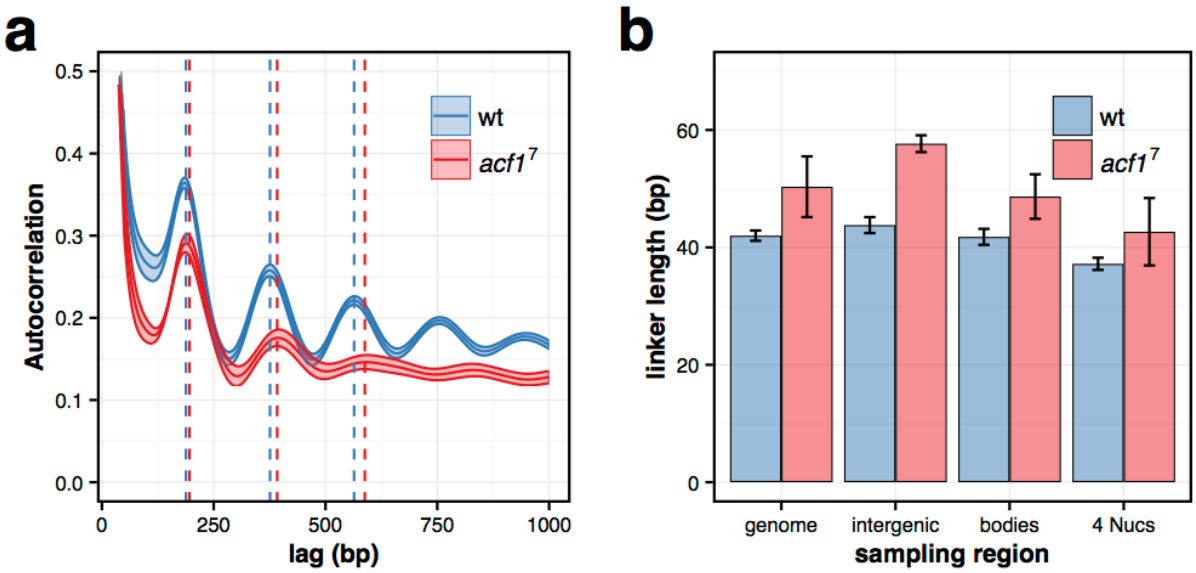

Figure 5: ACF1 endows euchromatin with periodicity and restricts linker lengths. (a) Changes in nucleosome periodicity on chromosomes 2 and 3 are estimated using the autocorrelation function. The correlation coefficients for the nucleosome occupancy values are plotted against the relative shifts. The mean and SEM of replicate samples are displayed. Dashed lines indicate the centers of nucleosome positions derived from the autocorrelation peaks. (b) Autocorrelation was used to estimate internucleosome linker lengths in various genomic regions across all experimental replicates. Error bars represent the SEM.

As ACF1 may affect nucleosome positioning or spacing differently at different parts of the genome, we calculated the autocorrelation coefficients selectively for gene bodies, intergenic regions or for the first 4 nucleosomes downstream of TSSs (Supplementary Fig. 4a). In these cases dyad density profiles along the respective genomic regions (e.g. TSSs) were concatemerized head to tail. ACF1 depletion caused a decay of regularity within gene bodies or intergenic regions as it did for the entire genome. Interestingly, the regular spacing of the first 4 nucleosomes downstream of TSS was not much affected by ACF1 deletion. This suggests that while ACF1 contributes to the bulk of nucleosome spacing in the genome, it does not affect the phasing at TSS, where other remodelers are known to be involved (Yen et al. 2012; Gkikopoulos et al. 2011).

The maxima in the autocorrelation curves indicate the spacing between adjacent nucleosomes, which can be used to determine the average NRL or the average lengths of the nucleosomal linker DNA (Fig. 5a). We used linear regression on the 2nd and 3rd maxima to calculate the linker lengths for all replicates across various sets of genomic features. The mean NRL for WT chromatin was determined to be 189 bp (which corresponds to a linker of 42 bp) (Fig. 5b). This compares well with the NRL values obtained by bulk MNase measurements (Lu et al. 2009; Braunschweig et al. 2009; Becker and Wu 1992). Similar analyses were carried out to determine NRLs as a function of gene length and expression strength in WT chromatin. Apparently, strongly expressed genes tend to have shorter linkers (42 bp) as compared to poorly expressed genes (51 bp), when the expression values were categorized into 4 equal-sized

groups. Furthermore, longer genes tend to have longer linkers (>4.2 kb long, 53 bp) than shorter genes (<1 kb long, 35 bp), possibly due to the contribution of introns in longer genes and relatively poor expression of long genes.

The calculations for the *acf1*^{7} mutant chromatin revealed an increased NRL from 189 bp to 197 bp. For intergenic regions the increase in NRL was most pronounced, from an average of 190 bp to 204 bp (Fig. 5b). The results of the autocorrelation analyses are not biased by any presumed differences in fragment length distribution in the sequencing libraries as the calculations were performed on computationally selected fragments below 200 bp. Subjecting fragments of different sizes to similar analyses yielded the same trend of array dampening and shift (Supplementary Fig. 4b). However, the amplitudes of the autocorrelation function depend on the library size (Supplementary Fig. 4c). The numbers of reads derived from the mutant sequencing libraries are lower than those in derived from WT libraries. To rule out that this difference leads to the observed dampening of periodicity in mutant chromatin, we randomly selected 19 million reads from each library and calculated the autocorrelation function. Indeed, the NRL shifts and dampening of amplitude in mutant chromatin were readily observed (Supplementary Fig. 4d).

In summary ACF1, and by inference the nucleosome sliding factors it defines, is involved in adjusting the distance between adjacent nucleosomes, which becomes remarkably larger in the absence of the remodeler.

Discussion

How regular is nucleosome spacing in euchromatin? Our idea of chromatin organization based on very regular successions of nucleosomes with defined spacing has been largely formed by pictures of DNA fragment ladders obtained by digestion of linker DNA in isolated nuclei with MNase and staining of bulk DNA with ethidium bromide (Blank et al. 1997; Becker and Wu 1992; Sun et al. 2001; Wallrath and Elgin 1995). Such analyses yield average values for nucleosome spacing, but recent genome-wide nucleosome mapping suggest that the succession of nucleosomes is less regular at individual loci (Mavrich et al. 2008). Nucleosome spacing is most defined downstream of active *Drosophila* promoters, but even these phased arrays are short and regularity is lost after a few nucleosomes. Nucleosomes just upstream of the very same promoter boundaries are much less regular. Conceivably, the MNase digestions patterns that visualize bulk chromatin are largely dominated by heterochromatin, which may be much more regular than active euchromatin (Valouev et al. 2011; Wallrath and Elgin 1995), where regulatory elements are abundant and chromatin is often disrupted by transcription (Deal et al. 2010).

In order to explore the degree of regularity in euchromatin we applied two bioinformatic approaches, spectral density estimation and autocorrelation, to interpret nucleosome occupancy profiles obtained by standard MNase-seq methodology (Wal and Pugh 2012). Although these methods have been used in a few cases (Jin et al. 2016; Braunschweig et al. 2009; Lantermann et al. 2010; Valouev et al. 2011), they are not routinely applied. Both methods reveal periodicity of nucleosomal arrangements relative to the underlying DNA sequence, allowing to assess regularity at different regions of the euchromatin in

Drosophila embryos. Both analytic methods interpret nucleosome positions relative to each other and their occupancy values, at large. Our analysis led to three novel findings. First, we systematically identified phased nucleosome arrays with regular spacing (PNA) at positions other than transcription start sites. Second, we extract information about the nucleosome repeat lengths at various euchromatin regions. Finally, by evaluating these euchromatin features in embryos lacking ACF1, the defining subunit of the two nucleosome sliding factors ACF and CHRAC, we reveal the involvement of these remodelers in nucleosome spacing.

The NRL is commonly derived from carefully measuring the lengths of fragments derived from partial MNase digestion of entire nuclei. In contrast to this determination of the genome-average NRL, the autocorrelation function can be applied to particular aspects of euchromatin, such as coding or intergenic regions. Our findings that the NRL differs in different parts of euchromatin highlights the flexibility of chromatin organization. Widely different bulk NRL have previously been found for different organisms and even different cell types of one organism (Teif et al. 2012; Valouev et al. 2011; Sperling and Weiss 1980; Sperling et al. 1980; Omori et al. 1980; Berkowitz and Riggs 1981; Jakob et al. 1984). Prevalent deviations from regular nucleosome spacing are likely to be accommodated if the fiber folds by interdigitation of nucleosomes in neighboring fibers (Maeshima et al. 2016).

Comparison of WT and mutant chromatin revealed a role for ACF1-containing nucleosome remodeling complexes as euchromatic nucleosome spacing factors, which is in line with the well-documented nucleosome spacing activity of CHRAC and ACF *in vitro* (Alexiadis et al. 1998; Ito et al. 1997; He et al. 2006). ACF has also been suggested to collaborate with histone chaperones for nucleosome assembly (Torigoe et al. 2011; Hwang et al. 2014; Ito et al. 1997; Varga-Weisz et al. 1997). Although the ChIP-seq analysis did not point to obvious differences in nucleosome density in the *acf1* mutants, is possible that reduced regularity stems from combined nucleosome spacing and assembly functions of ACF1. The regularity of nucleosomal arrays was much reduced in most parts of euchromatin in the absence of ACF1, with the notable exception of PNAs at TSS, where ACF1 did not affect the phasing of nucleosomes. Apparently, nucleosomes of promoter NDRs are placed by other remodelling enzymes in the context of transcription activation (Mavrich et al. 2008; Yen et al. 2012; Iyer 2012; Ganguli et al. 2014; Struhl and Segal 2013; Lieleg et al. 2015a), among them the ISWI-containing NURF (Kwon et al. 2016b). Several examples for roles for ISWI-type remodelers in phasing nucleosomes in the context of transcription initiation have also recently been described for vertebrates (Wiechens et al. 2016; Fennessy and Owen-Hughes 2016). These findings highlight the earlier notion that remodeling ATPases are harnessed for particular functions by associated complex subunits and that ACF1 instructs ISWI to different tasks (Mueller-Planitz et al. 2013; Clapier and Cairns 2009). In the context of the current study, the unaltered PNA downstream of TSS serve as convenient internal controls for our further findings.

The reduced regularity of chromatin in *acf1* mutant embryos was accompanied by a global increase of linker length in euchromatin. An earlier study had observed a reduced NRL in *acf1* mutant embryo chromati (Fyodorov et al. 2004). The discrepancy to our findings may be due to a difference in genotype. Fyodorov et al. had based their analysis on the $acf1^{1}$ mutant, which recently was shown not to be a clear loss-of-function mutant since it may express a stray C-terminal fragment of ACF1 (Börner et al. 2016).

Our current analysis was done on the *acf1*^{7} allele, which to the best of our knowledge is a null allele (Börner et al. 2016). On the other hand, the MNase analyses of Fyodorov and colleagues measured the bulk NRL, which may be dominated by heterochromatin. It is possible that the absence of ACF1 leads to increased NRL in euchromatin and decreased NRL in heterochromatin. In any case, deviations in NRL from wildtype in either *acf1* mutant are associated with 'sloppy' heterochromatin and chromatin-mediated silencing (Fyodorov et al. 2004; Chioda et al. 2010) and defects in cell specification (Börner et al. 2016).

The regularity of nucleosome arrays can be best appreciated if an array is phased with respect to a chromatin boundary. Well-described boundaries are TSS (Struhl and Segal 2013; Valouev et al. 2011; Teif et al. 2012; Mavrich et al. 2008), CTCF and insulator sites (Kwon et al. 2016b; Wiechens et al. 2016) and nucleosome phasing has also been reported at splice sites (Snyder et al. 2016). We employed spectral density estimation (SDE) to systematically search for PNAs. SDE does not rely on prior knowledge or annotation of genomic reference sites and thus is suited for *de novo* discovery of chromatin boundaries. About half of the PNAs detected by SDE correspond to TSS-associated arrays and a further 15% are explained by the presence of insulator proteins, which are not affected by ACF1 depletion.

ACF1-dependent PNAs (adPNA) are phased with respect to a novel ATACG motif in the central linker of the array. The apparent specificity of ACF1 for ATACG-sites may be due to recruitment of ACF1-containing enzymes by factors bound to these sites. Unfortunately, attempts to demonstrate any specific interaction of ACF1 with chromatin have been unsuccessful (Jain et al. 2015). Interestingly, we do not observe an extended region of nucleosome depletion (NDR) around ATACG motifs. This is in contrast to array formations around insulator binding sites and promoters and might indicate a peculiar principle of sequence-based arrays formation.

In the absence of evidence for a recruitment model we also consider an alternative explanation. The autocorrelation revealed a rather global role for ACF1 in adjusting NRLs throughout euchromatin. It is conceivable that CHRAC/ACF establish a ground state of regularity throughout euchromatin after replication, which is subsequently modulated, refined and disrupted by chromatin transcription and repair. The original effect of ACF1-mediated spacing may only be visible at those sites that are not extensively remodeled by such processes. The observation that adPNA sites are mainly located in inactive, state-9 chromatin is consistent with such a scenario. PNAs are prominent points of reference to study the placement of nucleosomes after replication at sites that are distinct from promoters (Ramachandran and Henikoff 2016; Fennessy and Owen-Hughes 2016). Applying SDE and autocorrelation to nucleosome positioning data from other species promises to identify further hallmarks of chromatin organisation.

Materials and Methods

Nucleosome mapping

Two *Drosophila melanogaster* genotypes (*w1118*, *yw*) that are wild type (WT) with respect to the ACF1 gene were used to establish reference maps of nucleosome positions. Three biological replicates (*w1118*, *acf1*^{7}) or 2 replicates (*yw*) were sequenced. The analyses were performed by comparing *acf1*^{7} against the combined WT profiles. Since the mutant flies are not backcrossed to any of the reference genotypes, their combined use should allow identifying ACF1-mediated effects more robustly.

For mapping nucleosomes embryos were collected 2-8 hr after egg laying, a developmental period of broad ACF1 expression (Chioda et al. 2010). One gram embryos were dechorionated in 120 ml 1:5 diluted sodium hypochloride (VWR, Cat.no. 301696S) for 3 min, thoroughly washed and fixed in 10 ml fixing solution [0.1 M NaCl, 0.05 M HEPES pH 8.0, 1 mM EDTA, 0.5 mM EGTA, 1.8% Formaldehyde (FA; Sigma, Cat. No F1635) added to 30 ml n-Heptane (VWR, Cat. No. 8.22332.1000)] for 15 min at 16-18°C on a rotating wheel. Fixation was quenched by adding 125 mM glycine. The embryos were subsequently washed with PBS (including 0.01% Triton-X100) for 10 min and stored at -80°C.

For nuclei isolation, embryos were slowly thawed and dounced using a glass homogenizer (Schubert, Cat.no. 9164693) with 20 strokes each of the A and B pestles in ice-cold NX-I buffer [15 mM HEPES pH 7.6, 10 mM KCl, 2 mM MgCl2, 0.5 mM EGTA, 0.1 mM EDTA, 350 mM sucrose, 1 mM DTT, 0.2 mM PMSF, Protease inhibitors Leupeptin, Pepstatin and Aprotinin (10 μg/ml)]. The lysate was filtered through Miracloth and nuclei were pelleted at 3,500 rpm, 10 min at 4°C.

For MNase digestion, the nuclei were suspended in the MNase digestion buffer. About 80 mg of nuclei were digested with 13 units of MNase (Sigma, Cat.no N5386) for 15 min, 37°C while shaking at 500 rpm in 1 ml volume. The reaction was stopped by adding 20 μl of 0.5 M EDTA, pH 8.0 and the tubes were quickly transferred to ice for 1 min. Nuclei were spun at 12,500 rpm, 10 min at 4°C. The supernatants containing most of the DNA were collected and the buffer composition was adjusted to RIPA [1% Triton X-100, 0.1% Na deoxycholate, 140 mM NaCl, 10 mM Tris pH 8.0, 1 mM EDTA, 0.1% SDS, 1mM PMSF]. The digestion predominantly yielded mononucleosomes (Fig. S1a)

Chromatin immunoprecipitation (ChIP) was performed by first pre-clearing the chromatin sample using a protein A+G (1:1) bead mix for 1 hr at 4°C. Then, 150 μl of chromatin was incubated overnight with 3.5 μl rabbit polyclonal anti-H3 antibody (Abcam, Cat.no ab1791) in a final volume of 500 μl. Nucleosomes were immunoprecipitated by adding a (1:1) mix of protein A+G beads for 3 hr at 4°C. Subsequently, the beads were washed 5 times in 1 ml RIPA buffer. Residual RNA was digested by RNase-A (10 μg/100 μl, Sigma, Cat. No. R4875) at 37°C for 20 min. Subsequent protein digestion (using 25 μg/100 μl, Proteinase K, Genaxxon, Cat.no. M3036.0100) and reversal of crosslinking were performed simultaneously at 68°C for 2 hr. DNA was purified using GenElute™ PCR Clean-Up Kit (Sigma, Cat.no NA1020).

Recovered DNA was quantified using the Qubit® dsDNA HS Assay Kit (Life Technologies, Cat.no.Q32851) and sequencing libraries were prepared using the MicroPlex Library Preparation kit

(Diagenode, Cat. No. C05010011) starting with 2 ng DNA whenever possible. PCR amplification was monitored by quantifying amplified libraries (maximum 19 cycles). The libraries were sequenced on a HighSeq 1500 (Illumina) instrument.

Chromatin Immunoprecipitation

For genome-wide mapping CTCF and H2A.V, chromatin was prepared from 0-12 hr old mixed sex Drosophila embryos using covaris sonication based shearing protocol as described earlier(Jain et al. 2015). For mapping of H2A.V, chromatin from 0-12 h old embryos was treated with MNase to obtain mononucleosomes as described above. We used rabbit α-CTCF (Moon et al. 2005) and rabbit α-H2A.V (generated by the Becker lab) in 1:40 dilution in 1:100 dilution for enriching the proteins of interest. Associated DNA was processed for sequencing as described above.

Nucleosome position data analysis

Paired-end reads were mapped to *D. melanogaster* genome version dm3 excluding the scaffold Uextra. We used Bowtie v1.1.1 with "-X 750" parameter setting. Dyad coverage vectors were obtained by size-selecting fragments of length >=120 and <=200 bp and resizing their length to 50 bp fixed at the fragment center, unless stated otherwise.

The results were robust against differences in sequencing library sizes as alternative data normalization methods to generate coverage vectors yielded similar outcomes. For instance, library size- or Z-score transformation- based normalization of coverage vectors obtained by reducing the sequenced fragments to 1 bp or 50 bp gave the same result (not shown).

Autocorrelation analysis

The autocorrelation function was calculated for the dyad coverage vectors obtained for the entire genome, gene bodies, first 4 nucleosomes or intergenic regions. The vectors for the last 3 cases represent head-to-tail concatemerized regions of given annotation considering their orientation. The function was run for the lag length of 1000 bp. Nucleosomal repeat lengths were obtained by linear regression of the first and second autocorrelation peak position with zero intercept. The slope of the regression was defined as repeat length, the linker length was derived by subtracting 146.

Spectral density estimation

For identifying PNA, the nucleosome signal along each chromosome was scanned in a sliding window of 1024 bp with a step of size 100 bp for a samples. In each window a periodogram was obtained using the R function spec.pgram with parameters log="n", pad=1, spans=c(3,3). The spectral density corresponding to a 193 bp period was extracted and log-transformed. PNAs were identified by averaging z-score transformed spectral densities of all wildtype samples and applying an arbitrary threshold of 2.5.

AdPNAs were identified as follows: we first determined PNAs in the mutant samples using the same approach as for WT. We then merged the PNAs of both conditions and removed regions <= 500 bp.

For each region and each sample we calculated the average z-score of spectral density. Differential regularity was then determined using a t-test on each region comparing average WT and mutant z-scores. P-values were adjusted using the using the Benjamini & Hochberg step-up FDR-controlling procedure. An FDR cutoff of 20% and a log fold difference < 0 was used to identify the regions of interest.

Motif analysis

We searched for enriched motifs in adPNA regions using MEME suite version 4.10.0 (Bailey et al. 2009) using the zero or one occurrence per sequence ("zoops"). Genome-wide searches for motif hits were performed with FIMO using a p-value cutoff of 1e-7.

Data Access

The next-generation sequencing data have been deposited at GEO under the accession GSE85407.

Acknowledgements

We thank and S. Krebs and H. Blum (LAFUGA at Gene Center, LMU, Munich) for outstanding sequencing service. This work was supported by the German Research Council (DFG) [CRC 1064/P01 to P.B.B., CRC 1064/Z04 to T.S.].

References

Alexiadis V, Varga-Weisz PD, Bonte E, Becker PB, Gruss C. 1998. In vitro chromatin remodelling by chromatin accessibility complex (CHRAC) at the SV40 origin of DNA replication. *EMBO J* **17**: 3428–3438.

Arnold CD, Gerlach D, Stelzer C, Boryn LM, Rath M, Stark A. 2013. Genome-Wide Quantitative Enhancer Activity Maps Identified by STARR-seq. *Science*.

Bailey TL, Boden M, Buske FA, Frith M, Grant CE, Clementi L, Ren J, Li WW, Noble WS. 2009. MEME SUITE: tools for motif discovery and searching. *Nucleic Acids Res* **37**: W202–8.

Becker PB, Workman JL. 2013. Nucleosome remodeling and epigenetics. *Cold Spring Harb Perspect Biol* **5**: a017905–a017905.

Becker PB, Wu C. 1992. Cell-free system for assembly of transcriptionally repressed chromatin from Drosophila embryos. *Mol Cell Biol* **12**: 2241–2249.

Berkowitz EM, Riggs EA. 1981. Characterization of rat liver oligonucleosomes enriched in transcriptionally active genes: evidence for altered base composition and a shortened nucleosome repeat. *Biochemistry* **20**: 7284–7290.

Blank TA, Sandaltzopoulos R, Becker PB. 1997. Biochemical analysis of chromatin structure and function using Drosophila embryo extracts. *Methods* **12**: 28–35.

Börner K, Jain D, Vazquez-Pianzola P, Vengadasalam S, Steffen N, Fyodorov DV, Tomancak P, Konev A, Suter B, Becker PB. 2016. A role for tuned levels of nucleosome remodeler subunit ACF1 during Drosophila oogenesis. *Dev Biol* **411**: 217–230.

Braunschweig U, Hogan GJ, Pagie L, van Steensel B. 2009. Histone H1 binding is inhibited by histone variant H3.3. *EMBO J* **28**: 3635–3645.

Celniker SE, Dillon LAL, Gerstein MB, Gunsalus KC, Henikoff S, Karpen GH, Kellis M, Lai EC, Lieb JD, MacAlpine DM, et al. 2009. Unlocking the secrets of the genome. *Nature* **459**: 927–930.

Chioda M, Vengadasalam S, Kremmer E, Eberharter A, Becker PB. 2010. Developmental role for ACF1-containing nucleosome remodellers in chromatin organisation. *Development* **137**: 3513–3522.

Clapier CR, Cairns BR. 2009. The biology of chromatin remodeling complexes. *Annu Rev Biochem* **78**: 273–304.

Comoglio F, Schlumpf T, Schmid V, Rohs R, Beisel C, Paro R. 2015. High-resolution profiling of Drosophila replication start sites reveals a DNA shape and chromatin signature of metazoan origins. *Cell Rep* **11**: 821–834.

Corona DF, Eberharter A, Budde A, Deuring R, Ferrari S, Varga-Weisz P, Wilm M, Tamkun J, Becker PB. 2000. Two histone fold proteins, CHRAC-14 and CHRAC-16, are developmentally regulated subunits of chromatin accessibility complex (CHRAC). *EMBO J* **19**: 3049–3059.

Cuddapah S, Jothi R, Schones DE, Roh T-Y, Cui K, Zhao K. 2009. Global analysis of the insulator binding protein CTCF in chromatin barrier regions reveals demarcation of active and repressive domains. *Genome Res* **19**: 24–32.

Deal RB, Henikoff JG, Henikoff S. 2010. Genome-wide kinetics of nucleosome turnover determined by metabolic labeling of histones. *Science* **328**: 1161–1164.

Fedor MJ, Lue NF, Kornberg RD. 1988. Statistical positioning of nucleosomes by specific protein-binding to an upstream activating sequence in yeast. *J Mol Biol* **204**: 109–127.

Fennessy RT, Owen-Hughes T. 2016. Establishment of a promoter-based chromatin architecture on recently replicated DNA can accommodate variable inter-nucleosome spacing. *Nucleic Acids Res* gkw331.

Fu Y, Sinha M, Peterson CL, Weng Z. 2008. The insulator binding protein CTCF positions 20 nucleosomes around its binding sites across the human genome. ed. B. Van Steensel. *PLoS Genet* **4**: e1000138.

Fyodorov DV, Blower MD, Karpen GH, Kadonaga JT. 2004. Acf1 confers unique activities to ACF/CHRAC and promotes the formation rather than disruption of chromatin in vivo. *Genes Dev* **18**: 170–183.

Gaffney DJ, McVicker G, Pai AA, Fondufe-Mittendorf YN, Lewellen N, Michelini K, Widom J, Gilad Y, Pritchard JK. 2012. Controls of nucleosome positioning in the human genome. *PLoS Genet* **8**: e1003036.

Ganguli D, Chereji RV, Iben JR, Cole HA, Clark DJ. 2014. RSC-dependent constructive and destructive interference between opposing arrays of phased nucleosomes in yeast. *Genome Res* **24**: 1637–1649.

Gilchrist DA, Adelman K. 2012. Coupling polymerase pausing and chromatin landscapes for precise regulation of transcription. *Biochim Biophys Acta* **1819**: 700–706.

Gkikopoulos T, Schofield P, Singh V, Pinskaya M, Mellor J, Smolle M, Workman JL, Barton GJ, Owen-Hughes T. 2011. A role for Snf2-related nucleosome-spacing enzymes in genome-wide nucleosome organization. *Science* **333**: 1758–1760.

Graveley BR, Brooks AN, Carlson JW, Duff MO, Landolin JM, Yang L, Artieri CG, van Baren MJ, Boley N, Booth BW, et al. 2011. The developmental transcriptome of Drosophila melanogaster. *Nature* **471**: 473–479.

Hartlepp KF, Fernández-Tornero C, Eberharter A, Grüne T, Müller CW, Becker PB. 2005. The histone fold subunits of Drosophila CHRAC facilitate nucleosome sliding through dynamic DNA interactions. *Mol Cell Biol* **25**: 9886–9896.

He X, Fan H-Y, Narlikar GJ, Kingston RE. 2006. Human ACF1 alters the remodeling strategy of SNF2h. *J Biol Chem* **281**: 28636–28647.

Hwang WL, Deindl S, Harada BT, Zhuang X. 2014. Histone H4 tail mediates allosteric regulation of nucleosome remodelling by linker DNA. *Nature* **512**: 213–217.

Igo-Kemenes T, Hörz W, Zachau HG. 1982. Chromatin. *Annu Rev Biochem* **51**: 89–121.

Ito T, Bulger M, Pazin MJ, Kobayashi R, Kadonaga JT. 1997. ACF, an ISWI-containing and ATP-utilizing chromatin assembly and remodeling factor. *Cell* **90**: 145–155.

Iyer VR. 2012. Nucleosome positioning: bringing order to the eukaryotic genome. *Trends Cell Biol* **22**: 250–256.

Jain D, Baldi S, Zabel A, Straub T, Becker PB. 2015. Active promoters give rise to false positive “Phantom Peaks” in ChIP-seq experiments. *Nucleic Acids Res* **43**: 6959–6968. http://eutils.ncbi.nlm.nih.gov/entrez/eutils/elink.fcgi?dbfrom=pubmed&id=26117547&retmode=ref&cmd=prlinks.

Jakob KM, Ben Yosef S, Tal I. 1984. Reduced repeat length of nascent nucleosomal DNA is generated by replicating chromatin in vivo. *Nucleic Acids Res* **12**: 5015–5024.

Jin H, Rube HT, Song JS. 2016. Categorical spectral analysis of periodicity in nucleosomal DNA. *Nucleic Acids Res* **44**: 2047–2057.

Kharchenko PV, Alekseyenko AA, Schwartz YB, Minoda A, Riddle NC, Ernst J, Sabo PJ, Larschan E, Gorchakov AA, Gu T, et al. 2011. Comprehensive analysis of the chromatin landscape in Drosophila melanogaster. *Nature* **471**: 480–485.

Krietenstein N, Wal M, Watanabe S, Park B, Peterson CL, Pugh BF, Korber P. 2016. Genomic Nucleosome Organization Reconstituted with Pure Proteins. *Cell* **167**: 709–721.e12.

Kukimoto I, Elderkin S, Grimaldi M, Oelgeschläger T, Varga-Weisz PD. 2004. The histone-fold protein complex CHRAC-15/17 enhances nucleosome sliding and assembly mediated by ACF. *Mol Cell* **13**: 265–277.

Kwon SY, Grisan V, Jang B, Herbert J, Badenhorst P. 2016a. Genome-Wide Mapping Targets of the Metazoan Chromatin Remodeling Factor NURF Reveals Nucleosome Remodeling at Enhancers, Core Promoters and Gene Insulators. ed. B. Hendrich. *PLoS Genet* **12**: e1005969.

Kwon SY, Grisan V, Jang B, Herbert J, Badenhorst P. 2016b. Genome-Wide Mapping Targets of the Metazoan Chromatin Remodeling Factor NURF Reveals Nucleosome Remodeling at Enhancers, Core Promoters and Gene Insulators ed. B. Hendrich. *PLoS Genet* **12**: e1005969–26.

Lantermann AB, Straub T, Stralfors A, Yuan G-C, Ekwall K, Korber P. 2010. Schizosaccharomyces pombe genome-wide nucleosome mapping reveals positioning mechanisms distinct from those of Saccharomyces cerevisiae. *Nat Struct Mol Biol* **17**: 251–257. http://www.nature.com/nsmb/journal/v17/n2/full/nsmb.1741.html.

Lieleg C, Ketterer P, Nuebler J, Ludwigsen J, Gerland U, Dietz H, Mueller-Planitz F, Korber P. 2015a. Nucleosome spacing generated by ISWI and CHD1 remodelers is constant regardless of nucleosome density. *Mol Cell Biol* **35**: 1588–1605.

Lieleg C, Krietenstein N, Walker M, Korber P. 2015b. Nucleosome positioning in yeasts: methods, maps, and mechanisms. *Chromosoma* **124**: 131–151.

Love MI, Huber W, Anders S. 2014. Moderated estimation of fold change and dispersion for RNA-seq data with DESeq2. *Genome Biol* **15**: 550.

Lu X, Wontakal SN, Emelyanov AV, Morcillo P, Konev AY, Fyodorov DV, Skoultchi AI. 2009. Linker histone H1 is essential for Drosophila development, the establishment of pericentric heterochromatin, and a normal polytene chromosome structure. *Genes Dev* **23**: 452–465.

Maeshima K, Rogge R, Tamura S, Joti Y, Hikima T, Szerlong H, Krause C, Herman J, Seidel E, DeLuca J, et al. 2016. Nucleosomal arrays self-assemble into supramolecular globular structures lacking 30-nm fibers. *EMBO J* **35**: 1115–1132.

Mathelier A, Zhao X, Zhang AW, Parcy F, Worsley-Hunt R, Arenillas DJ, Buchman S, Chen C-Y, Chou A, Ienasescu H, et al. 2014. JASPAR 2014: an extensively expanded and updated open-access database of transcription factor binding profiles. *Nucleic Acids Res* **42**: D142–7.

Mavrich TN, Jiang C, Ioshikhes IP, Li X, Venters BJ, Zanton SJ, Tomsho LP, Qi J, Glaser RL, Schuster SC, et al. 2008. Nucleosome organization in the Drosophila genome. *Nature* **453**: 358–362.

Moon H, Filippova G, Loukinov D, Pugacheva E, Chen Q, Smith ST, Munhall A, Grewe B, Bartkuhn M, Arnold R, et al. 2005. CTCF is conserved from Drosophila to humans and confers enhancer blocking of the Fab-8 insulator. *EMBO Rep* **6**: 165–170.

Mueller-Planitz F, Klinker H, Becker PB. 2013. Nucleosome sliding mechanisms: new twists in a looped history. *Nat Struct Mol Biol* **20**: 1026–1032.

Narlikar GJ, Sundaramoorthy R, Owen-Hughes T. 2013. Mechanisms and functions of ATP-dependent chromatin-remodeling enzymes. *Cell* **154**: 490–503.

Omori A, Igo-Kemenes T, Zachau HG. 1980. Different repeat lengths in rat satellite I DNA containing chromatin and bulk chromatin. *Nucleic Acids Res* **8**: 5363–5375.

Peterson CL, Almouzni G. 2013. Nucleosome dynamics as modular systems that integrate DNA damage and repair. *Cold Spring Harb Perspect Biol* **5**: a012658–a012658.

Poot RA, Dellaire G, Hülsmann BB, Grimaldi MA, Corona DF, Becker PB, Bickmore WA, Varga-Weisz PD. 2000. HuCHRAC, a human ISWI chromatin remodelling complex contains hACF1 and two novel histone-fold proteins. *EMBO J* **19**: 3377–3387.

Ramachandran S, Henikoff S. 2016. Transcriptional Regulators Compete with Nucleosomes Post-replication. *Cell* **165**: 580–592.

Sala A, Toto M, Pinello L, Gabriele A, Di Benedetto V, Ingrassia AMR, Bosco Lo G, Di Gesù V, Giancarlo R, Corona DFV. 2011. Genome-wide characterization of chromatin binding and nucleosome spacing activity of the nucleosome remodelling ATPase ISWI. *EMBO J* **30**: 1766–1777.

Sexton T, Yaffe E, Kenigsberg E, Bantignies F, Leblanc B, Hoichman M, Parrinello H, Tanay A, Cavalli G. 2012. Three-dimensional folding and functional organization principles of the Drosophila genome. *Cell* **148**: 458–472.

Siepel A, Bejerano G, Pedersen JS, Hinrichs AS, Hou M, Rosenbloom K, Clawson H, Spieth J, Hillier LW, Richards S, et al. 2005. Evolutionarily conserved elements in vertebrate, insect, worm, and yeast genomes. *Genome Res* **15**: 1034–1050.

Snyder MW, Kircher M, Hill AJ, Daza RM, Shendure J. 2016. Cell-free DNA Comprises an In Vivo Nucleosome Footprint that Informs Its Tissues-Of-Origin. *Cell* **164**: 57–68.

Soboleva TA, Nekrasov M, Ryan DP, Tremethick DJ. 2014. Histone variants at the transcription start-site. *Trends Genet* **30**: 199–209.

Sperling L, Tardieu A, Weiss MC. 1980. Chromatin repeat length in somatic hybrids. *Proc Natl Acad Sci USA* **77**: 2716–2720.

Sperling L, Weiss MC. 1980. Chromatin repeat length correlates with phenotypic expression in hepatoma cells, their dedifferentiated variants, and somatic hybrids. *Proc Natl Acad Sci USA* **77**: 3412–3416.

Struhl K, Segal E. 2013. Determinants of nucleosome positioning. *Nat Struct Mol Biol* **20**: 267–273.

Sugiyama T, Cam HP, Sugiyama R, Noma K-I, Zofall M, Kobayashi R, Grewal SIS. 2007. SHREC, an effector complex for heterochromatic transcriptional silencing. *Cell* **128**: 491–504.

Sun FL, Cuaycong MH, Elgin SC. 2001. Long-range nucleosome ordering is associated with gene silencing in Drosophila melanogaster pericentric heterochromatin. *Mol Cell Biol* **21**: 2867–2879.

Szerlong HJ, Hansen JC. 2011. Nucleosome distribution and linker DNA: connecting nuclear function to dynamic chromatin structure. *Biochem Cell Biol* **89**: 24–34.

Teif VB, Vainshtein Y, Caudron-Herger M, Mallm J-P, Marth C, Höfer T, Rippe K. 2012. Genome-wide nucleosome positioning during embryonic stem cell development. *Nat Struct Mol Biol* **19**: 1185–1192.

Torigoe SE, Urwin DL, Ishii H, Smith DE, Kadonaga JT. 2011. Identification of a rapidly formed nonnucleosomal histone-DNA intermediate that is converted into chromatin by ACF. *Mol Cell* **43**: 638–648.

Tsukiyama T, Daniel C, Tamkun J, Wu C. 1995. ISWI, a member of the SWI2/SNF2 ATPase family, encodes the 140 kDa subunit of the nucleosome remodeling factor. *Cell* **83**: 1021–1026.

Tsukiyama T, Wu C. 1995. Purification and properties of an ATP-dependent nucleosome remodeling factor. *Cell* **83**: 1011–1020.

Valouev A, Johnson SM, Boyd SD, Smith CL, Fire AZ, Sidow A. 2011. Determinants of nucleosome organization in primary human cells. *Nature* **474**: 516–520.

Varga-Weisz PD, Wilm M, Bonte E, Dumas K, Mann M, Becker PB. 1997. Chromatin-remodelling factor CHRAC contains the ATPases ISWI and topoisomerase II. *Nature* **388**: 598–602.

Wal M, Pugh BF. 2012. Genome-wide mapping of nucleosome positions in yeast using high-resolution MNase ChIP-Seq. *Meth Enzymol* **513**: 233–250.

Wallrath LL, Elgin SC. 1995. Position effect variegation in Drosophila is associated with an altered chromatin structure. *Genes Dev* **9**: 1263–1277.

Weber CM, Henikoff S. 2014. Histone variants: dynamic punctuation in transcription. *Genes Dev* **28**: 672–682.

Wiechens N, Singh V, Gkikopoulos T, Schofield P, Rocha S, Owen-Hughes T. 2016. The Chromatin Remodelling Enzymes SNF2H and SNF2L Position Nucleosomes adjacent to CTCF and Other Transcription Factors. ed. P. Varga-Weisz. *PLoS Genet* **12**: e1005940.

Yen K, Vinayachandran V, Batta K, Koerber RT, Pugh BF. 2012. Genome-wide nucleosome specificity and directionality of chromatin remodelers. *Cell* **149**: 1461–1473.

Zlatanova J, Leuba SH, van Holde K. 1999. Chromatin structure revisited. *Crit Rev Eukaryot Gene Expr* **9**: 245–255.